AD-A092 699 MASSACHUSETTS INST OF TECH LEXINGTON LINCOLN LAB F/G 20/12
ELECTROOPTICAL DEVICES.(U)
MAR 80 C E HURWITZ F19628-80-C-0002
UNCLASSIFIED ESD-TR-80-168 NL

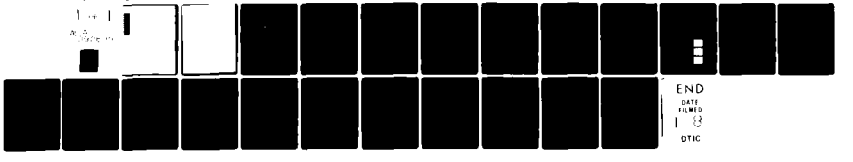

END
DATE FILMED
8
DTIC

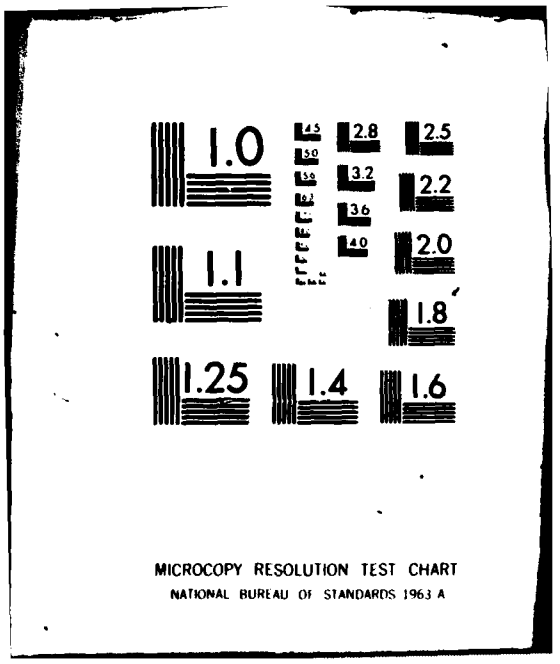
1.0
1.1
1.25
1.4
1.6
1.8
2.0
2.2
2.5
2.8
3.2
3.6
4.0
4.5
5.0
5.6
6.3
MICROCOPY RESOLUTION TEST CHART
NATIONAL BUREAU OF STANDARDS 1963 A

DISCLAIMER NOTICE

THIS DOCUMENT IS BEST QUALITY PRACTICABLE. THE COPY FURNISHED TO DTIC CONTAINED A SIGNIFICANT NUMBER OF PAGES WHICH DO NOT REPRODUCE LEGIBLY.

MASSACHUSETTS INSTITUTE OF TECHNOLOGY
LINCOLN LABORATORY

ELECTROOPTICAL DEVICES

SEMIANNUAL TECHNICAL SUMMARY REPORT
TO THE
ROME AIR DEVELOPMENT CENTER

1 OCTOBER 1979 – 31 MARCH 1980

ISSUED 22 OCTOBER 1980

LEXINGTON MASSACHUSETTS

ABSTRACT

This report covers work carried out with support of the Department of the Air Force during the period 1 October 1979 through 31 March 1980. A part of this support was provided by the Rome Air Development Center.

CW operation at temperatures up to 55°C has been achieved for GaInAsP/InP double-heterostructure (DH) lasers emitting at 1.5 μm, which were grown without a GaInAsP buffer layer. These devices are of interest for use as sources in fiber-optics communications systems, since the lowest transmission loss reported for fused-silica optical fibers occurs at 1.55 μm.

Surface passivation techniques developed for InP and GaInAsP avalanche photodiodes have resulted in reductions of dark current as large as four orders of magnitude, to values as low as 1.6×10^{-6} A/cm^2 at 0.9 V_b, where V_b is the breakdown voltage. Devices consisting entirely of InP have been passivated with plasma-deposited Si_3N_4, and those with a GaInAsP layer but with the p-n junction in InP have been passivated with polyimide. Neither of these techniques successfully reduces dark currents in devices with the p-n junction in the GaInAsP, but a film of photoresist sprayed with SF_6 as the propellant has given excellent results.

The electrical characteristics of InP ion implanted with Sn, Ge, Si, and C have been investigated. All of these column IV elements yielded n-type conductivity and Sn, Ge, and Si showed high electrical activation; however, implanted C was found to have a net electrical activation of only about 5 percent.

The growth-temperature dependence of the GaInAsP/InP lattice mismatch has been measured over a wide range of quaternary compositions. Smooth GaInAsP layers have been grown directly on InP substrates without an InP buffer layer; however, the use of an InP layer results in a smooth GaInAsP/InP interface, which is needed for DH lasers.

CONTENTS

ELECTROOPTICAL DEVICES

I. HIGH-TEMPERATURE CW OPERATION OF GaInAsP/InP LASERS EMITTING AT 1.5 μm

The lowest transmission loss reported[1] for fused-silica optical fibers, 0.2 dB/km, has been obtained at 1.55 μm. Consequently, there is strong current interest in the development of diode lasers emitting at ~1.5 μm for use as sources in fiber-optics communications systems. In this section we report the fabrication of GaInAsP/InP double-heterostructure (DH) lasers emitting in this wavelength region that have been operated CW at heat-sink temperatures as high as 55°C. Although room-temperature CW operation of 1.5-μm GaInAsP/InP lasers has been described recently,[2-5] CW operation of these devices at temperatures above 20°C has not been reported. The high-temperature capability of the present lasers is significant not only because it would permit system operation above room temperature if desirable, but also because longer lifetimes for room-temperature operation can be expected for devices with this capability. For the laser with the best room-temperature characteristics, the CW threshold current I_{th} was 120 mA and the external differential quantum efficiency η_d was 28 percent. These values are comparable to those obtained for GaInAsP/InP DH lasers emitting at 1.1 to 1.3 μm (Ref. 6) and significantly better than the best room-temperature values (I_{th} = 150 mA, η_d = 19 percent) previously obtained[4] for 1.5-μm devices.

The heterostructures used for conventional GaInAsP/InP DH lasers emitting at 1.1 to 1.3 μm consist of successive InP, GaInAsP, and InP layers grown by liquid-phase epitaxy (LPE) at 630° to 650°C on InP substrates. The thickness of the GaInAsP active layer is of the order of 0.1 μm. Considerable difficulty is encountered in using the same structure and growth procedure for 1.5-μm lasers because the P content in the thin active layer is so low that there is a strong tendency for this layer to be dissolved by the growth solution used for deposition of the upper InP layer. In fabricating the 1.5-μm lasers reported previously, the dissolution problem was solved either by lowering the LPE growth temperature for the upper InP layer to 592°C (Ref. 2) in order to reduce the solubility of the active layer in the InP growth solution, or by growing a GaInAsP buffer layer between the active layer and the upper InP layer, using an intermediate composition for the buffer layer such that its growth solution did not dissolve the active layer.[3-5] Neither of these methods was employed in preparing the lasers described here. Instead, conventional three-layer heterostructures were obtained by LPE growth at 640°C (Ref. 7), but dissolution was prevented by supercooling the growth solution for the upper InP layer by 10° to 12°C before placing it in contact with the active layer.

We have used Auger spectroscopy in combination with ion-beam sputtering to analyze one of the heterostructures grown by the supercooling technique. The approximately 0.4-μm-thick active layer was found to have a symmetrical composition profile, with a central region of uniform composition bordered at the top and bottom by transition regions each about 0.05 μm thick in which the composition changed gradually to that of InP. The dependence of composition on distance was similar in these two regions. Since dissolution of the lower InP layer does not occur during the growth of the GaInAsP active layer, the similarity in the composition gradients indicates that dissolution of the active layer did not occur during growth of the upper InP layer.

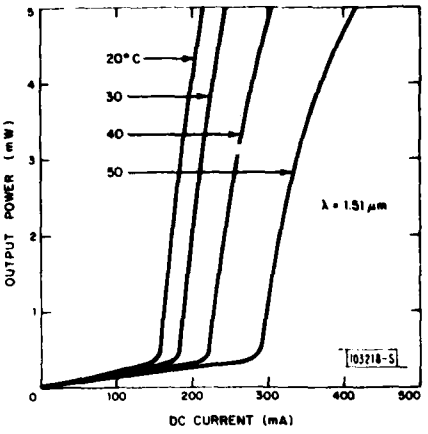

Fig. I-1. Light output vs current for CW operation of GaInAsP/InP laser emitting at 1.51 μm.

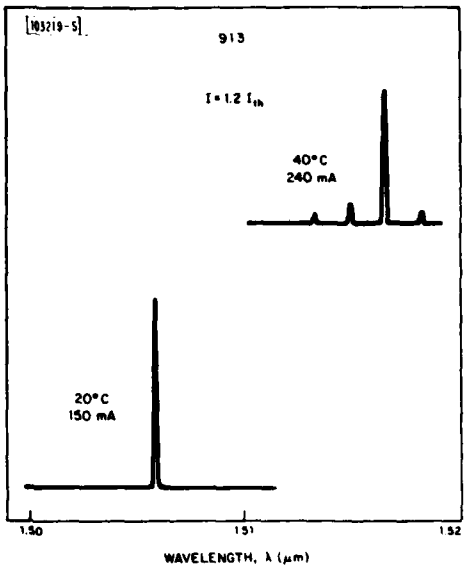

Fig. I-2. Emission spectra for GaInAsP/InP laser at 20° and 40°C.

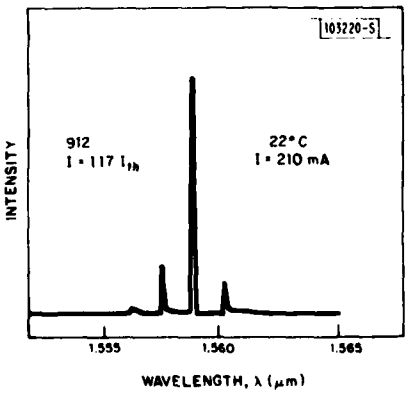

Fig. I-3. Emission spectrum for GaInAsP/InP laser at 22°C.

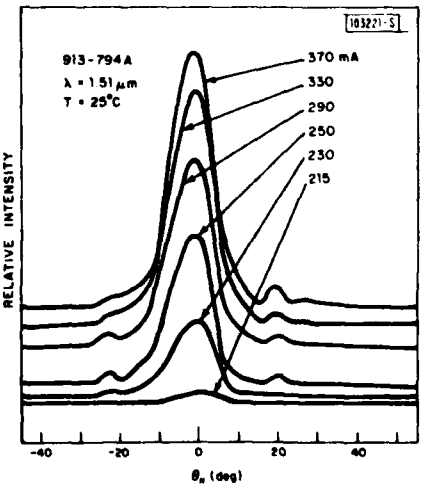

Fig. I-4. Far-field patterns as a function of current for GaInAsP/InP laser emitting at 1.51 μm.

The CW lasers were fabricated from heterostructures in which all three epitaxial layers were n-type, and stripes were defined by the deep-Zn-diffusion technique used previously for shorter-wavelength devices.[6] Figure I-1 shows the curves of light output vs current measured for CW operation of one laser at 20°, 30°, 40°, and 50°C. At 20°C, where the emission wavelength was 1.51 μm, I_{th} = 150 mA and η_d = 13 percent. For this device, I_{th} is approximately proportional to $\exp[-T/T_o]$, with T_o = 53°C near room temperature, in good agreement with previous results for pulsed operation.[4] The maximum CW operating temperature was 55°C, the highest value we have achieved for 1.5-μm lasers.

Figure I-2 shows the emission spectra obtained for 20° and 40°C operation of another CW laser at about 20 percent above threshold. The emission peak moves from 1.506 Å at 20°C to 1.517 Å at 40°C, a shift of 5.5 Å/deg. Figure I-3 shows the emission spectrum obtained for 22°C operation of a third laser at 17 percent above threshold, where the emission peak occurs at 1.559 μm. The lasers of Figs. I-2 and -3 were fabricated from two different wafers. The composition of the growth solution for the active layer was the same in both cases, but the active layer thicknesses were 0.1 and 0.4 μm, respectively.

For all the CW lasers tested, a single longitudinal mode was predominant, as shown by the spectra of Figs. I-2 and -3. Figure I-4 shows the far-field patterns as a function of current for a second laser fabricated from the same wafer as the device of Fig. I-2. These patterns show single transverse mode operation up to the highest current used, about 70 percent above threshold, where the output exceeded 10 mW/facet.

In addition to characterizing the CW operation of stripe-geometry lasers, we have also investigated the pulsed operation of broad-area 1.5-μm lasers, which were fabricated from wafers with an as-grown p-type InP top layer. The values of threshold current density J_{th} are comparable to those broad-area lasers emitting at 1.1 to 1.3 μm (Ref. 8). The best value of J_{th}, 1.7 kA/em^2, normalized to a cavity length of 250 μm, is the lowest value so far reported for 1.5-μm lasers. For diodes from substantial areas of each wafer, however, laser action did not occur even at current densities up to 20 kA/cm^2. This inhomogeneity suggests that at least partial dissolution of the active layer may have occurred in those areas which did not yield laser diodes.

J. J. Hsieh

II. SURFACE PASSIVATION TECHNIQUES FOR InP AND GaInAsP/InP p-n JUNCTION STRUCTURES

In this section we report on the use of three materials, plasma-deposited Si_3N_4, polyimide and SF_6-propelled photoresist, to passivate etched-mesa avalanche photodiodes (APDs) in InP and GaInAsP. Three different structures were investigated: n-InP/p^+-InP, n^+-InP/n-GaInAsP/n-InP/p^+-InP, and n^+-InP/n-GaInAsP/p^+-InP. With the appropriate choice of passivation technique for a given structure, substantial reductions in dark current have been obtained.

Plasma-deposited Si_3N_4 was found to be a simple and effective passivation for the first structure, n-InP/p^+-InP inverted-mesa APDs (Ref. 9). These devices were fabricated from wafers consisting of a layer of n-InP ($n \sim 3 \times 10^{16}$ cm^{-3}) grown by LPE on p^+-InP substrates. 170-μm-diameter mesas were etched using a 1:1 mixture of 3% Br-methanol:H_3PO_4 at 45°C. Figure II-1(a) shows the reverse I-V characteristic of one of these diodes after etching and with no surface passivation. The I-V characteristic was very "soft" and the leakage current at 45 V was over 90 μA. Figures II-1(b) and (c) show the I-V characteristics of the same diode after the application of a 900-Å-thick layer of Si_3N_4 by the pyrolytic reaction of SiH_4 and N_2 in a RF plasma at a substrate temperature of 250°C. A film thickness of 900 A was chosen on the basis of its use as an antireflection coating. The diode now has a sharp breakdown at 46 V and a dark current of 12 nA at 45 V. These diodes typically exhibited dark current densities of 2×10^{-5} A/cm^2 at 0.9 V_b, where V_b is the breakdown voltage. As indicated in these photographs, the Si_3N_4 passivation resulted in a decrease of the leakage current near breakdown of nearly four

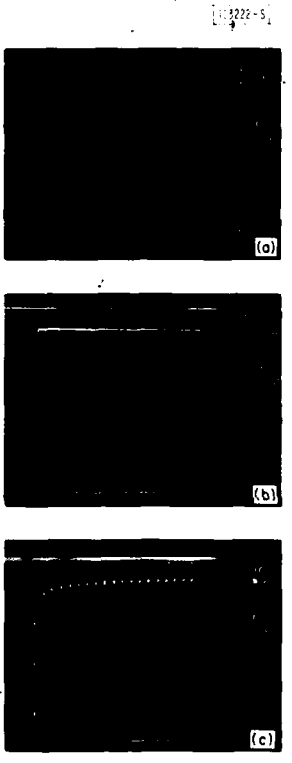

Fig. II-1. Reverse I-V characteristics for a p^+-n InP avalanche photodiode. Horizontal scale: 5 V/div. (a) Before Si_3N_4 passivation, 10 A/div; (b) after Si_3N_3 passivation, 1 A/div; and (c) after Si_3N_4 passivation, 10 nA/div.

orders of magnitude. Preliminary tests indicate that the polyimide coating, described below, yields comparable results. However, Si_3N_4 offers the advantage of easy removal over the fully polymerized polyimide, which can only be removed by plasma ashing.

The other two structures for which passivating coatings were studied were both GaInAsP/InP avalanche photodiodes with a long wavelength cutoff of about 1.3 μm. They were also etched mesa devices fabricated in the same manner as the InP APDs. One device, in which extremely promising detector performance has been obtained,[10,11] actually has the p-n junction in the InP and a depletion layer which, at high bias, extends into the GaInAsP. The same Si_3N_4 passivating film described above and successfully used with all-InP devices was found to be unsatisfactory for these heterostructures. Although reasonably low leakage current densities (5×10^{-4} A/cm^2 at 0.9 V_b) were obtained initially,[10] a marked degradation in device performance was observed when the devices were exposed to high humidity or sustained high bias (~0.9 V_b for ~1 min.). The sensitivity to atmospheric moisture was reduced by adding a sealing layer of fully cured photoresist* (PR) to the Si_3N_4-covered devices; however, the bias-induced degradation remained. A passivating coating which was found to be highly effective is a polyimide (PI) film† (5 to 8 μm thick) applied directly over the freshly etched mesas. The PI film was deposited and patterned using standard photolithographic techniques and was polymerized by baking at 120° and 200°C for 1 hr each. Further baking or higher temperatures resulted in degraded device characteristics, possibly due to dopant impurity diffusion. When the above procedures were used, the PI-passivated devices exhibited no current increase with sustained bias. Leakage current densities as low as 1.6×10^{-6} A/cm^2 at 0.9 V_b were measured.

Devices of the third type,[12] with the p-n junction at the InP-GaInAsP interface or in the GaInAsP layer, exhibited high leakage currents not only when uncoated, but also when passivated with either Si_3N_4 or PI. The surface-related nature of the leakage currents was confirmed by testing the uncoated devices in several gaseous environments (O_2, NH_4OH, and SF_6). In particular, when tested in an SF_6 atmosphere,[13] the devices showed a dramatic improvement in performance, exhibiting low leakage current and sharp breakdown. This effect might be attributed to the high electron affinity of SF_6, which tends to reduce excess surface charge, and to its high dielectric constant, which lowers fringing fields at the exposed junction. Unfortunately, the high value of leakage current returned when the device was removed from the SF_6 ambient.

In a separate experiment it was observed that when PR was applied immediately after etching the mesas, considerable improvement in the device characteristics was also obtained. Based upon these two observations, a method was developed in which SF_6 was used as the propellant gas for PR spraying, producing a surface coating that appears to combine the advantages of the PR passivation with those of the SF_6 ambient, but permits the operation of the device in air. Devices passivated in this manner exhibited current densities as low as 2×10^{-5} A/cm^2 at 0.9 V_b. The passivation effects were reversible upon removal and reapplication of the SF_6-propelled PR layer. The presence of this PR layer was found to have no adverse effect on the photoresponse of these devices.

V. Diadiuk S. H. Groves
C. A. Armiento C. E. Hurwitz

* Shipley AZ1350J positive photoresist.

† Dupont PI-255 polyimide coating for semiconductor fabrication.

III. ELECTRICAL CHARACTERISTICS OF InP IMPLANTED WITH COLUMN IV ELEMENTS

In this section we report results of a study on the electrical characteristics of InP implanted with the column IV elements from C to Sn, including new and more detailed data for Si in InP. Previous work[14-19] has dealt primarily with InP implanted with column II or column VI elements, whereas among the column IV elements, only Si has been investigated to any extent.[14,15,18,19]

High-resistivity ($\rho > 10^7$ Ω-cm), Fe-doped, (111)-oriented InP samples were used in these experiments. Following implantation, the samples were annealed at 750°C for 10 to 15 min. using a PSG (phosphosilicate glass) encapsulation technique described previously.[14] Details of the sample processing before and after implantation can be found in Refs. 14 and 17.

The sheet carrier concentrations and mobilities of InP samples implanted with 1×10^{14} cm^{-2} of 400-keV C, Si, Ge, and Sn are shown in Fig. III-1 as a function of implant temperature. Implantation of all these column IV elements resulted in layers showing n-type conductivity. As shown in Fig. III-1(a), however, data from the samples implanted with C indicate a low net electrical activation (about 5 percent) of the implanted C. Samples implanted with carbon doses ranging from 1×10^{13} cm^{-2} to 1×10^{15} cm^{-2} all show this same effect. These results indicate that C is likely highly amphoteric in InP, although other possibilities, such as the location of most of the carbon on interstitial sites, cannot be entirely ruled out. This behavior of implanted C in InP contrasts with that in GaAs, where implanted C was found to be p-type with up to 50 percent effective doping efficiency.[20]

Samples implanted with the other column IV elements, Si, Ge, and Sn, all showed n-type behavior with good electrical activation and a similar dependence on implantation temperature and dose. For these elements, sheet resistivities of InP samples implanted at temperatures of 150° to 200°C were generally lower than those of samples implanted at room temperature. The sheet mobilities were always higher for the elevated temperature implants, but several anomalies in the sheet carrier concentration as a function of implant temperature and dose were observed.

The results for 1×10^{14} cm^{-2} silicon implants are shown in Fig. III-1(b). Over the 25° to 200°C range of sample temperature during implantation, the sheet carrier concentration and mobility increased with increasing implant temperature. As indicated in the figure, there is considerable scatter in the room-temperature results with the measured sheet carrier concentrations ranging from 4.8×10^{13} to 7.0×10^{13} cm^{-2}. The room-temperature implanted samples with the higher sheet concentrations invariably had lower mobilities, so that even when the sheet concentrations were comparable to those on samples implanted at elevated temperatures, the sheet resistivities were always considerably higher. Since residual implant damage in InP has been shown to result in n-type conductivity with low mobility,[14] the variability of these room-temperature implant results indicate that Si is of an intermediate mass between light ions and heavy ions and that the damage created during room-temperature Si implantation into InP is critically dependent on the precise implant parameters.[21] The results on samples implanted with silicon at elevated temperatures were very reproducible. All samples implanted at 200°C with 1×10^{14} cm^{-2} had measured sheet carrier concentrations and mobilities in the range $(7.6 \text{ to } 7.8) \times 10^3$ cm^{-2} and (1800 to 2000) $cm^2/V\text{-sec}$, respectively.

For 1×10^{14} cm^{-2} germanium implants, the results on samples implanted at all temperatures were reproducible. As shown in Fig. III-1(c), higher sheet mobilities were obtained on

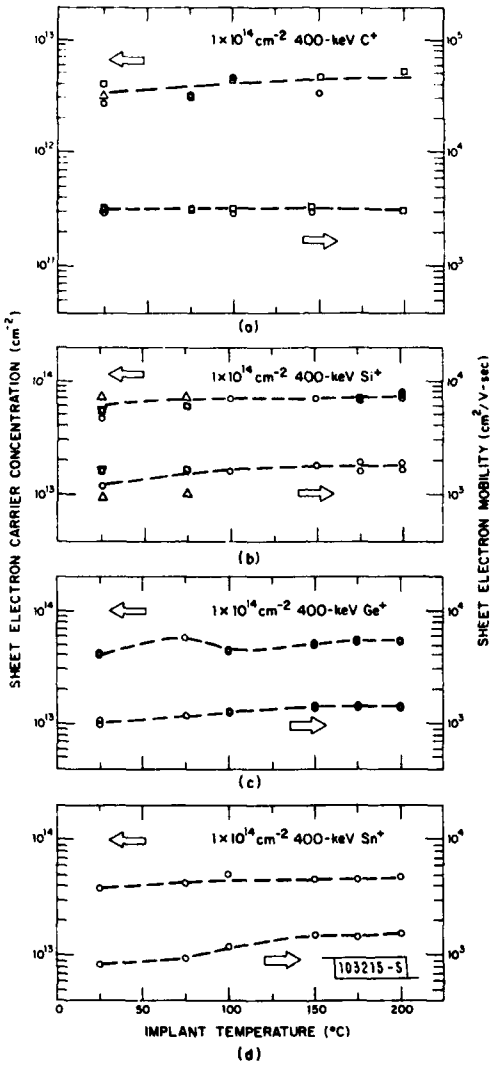

Fig. III-1. The sheet carrier concentration and mobilities vs implant temperature of InP samples implanted with 1×10^{14} cm^{-2} of 400 keV: (a) C, (b) Si, (c) Ge, and (d) Sn. All the samples were annealed at 750°C using a PSG encapsulation technique.

the sample implanted at 150° to 200°C. The sheet carrier concentrations measured on these samples were also higher than those obtained on similar samples implanted at room temperature, but as shown in the figure, there is an unexpected but reproducible anomalous peak in the sheet concentration for samples implanted at 75°C. The mobility measured on these samples (1100 to 1200 cm^2/V-sec), however, were sufficiently lower than on those implanted at 150° to 200°C, so that the higher-temperature implanted samples invariably had lower sheet resistivities. All the samples implanted at temperatures of 150° to 200°C with 1×10^{14} cm^{-2} of Ge exhibited measured sheet carrier concentrations and mobilities in the range (5.2 to 5.6) × 10^{13} cm^{-2} and (1480 to 1540) cm^2/V-sec, respectively.

Samples implanted with 1×10^{14} cm^{-2} of 400-keV Sn are shown in Fig. III-1(d). They are very similar to those obtained with Ge, except for the absence of the pronounced maximum in sheet carrier concentration. For samples implanted at 200°C, the measured sheet carrier concentrations and mobilities were typically 4.6×10^{13} cm^{-2} and 1450 cm^2/V-sec, respectively.

In contrast to the results discussed above, for Si, Ge, or Sn doses higher than about mid-10^{14} cm^{-2}, the sheet carrier concentrations measured on samples implanted at room temperature were higher than those measured on samples implanted at 150° to 200°C. This is illustrated in Fig. III-2, where the sheet electron concentration and mobility vs dose for InP sam-

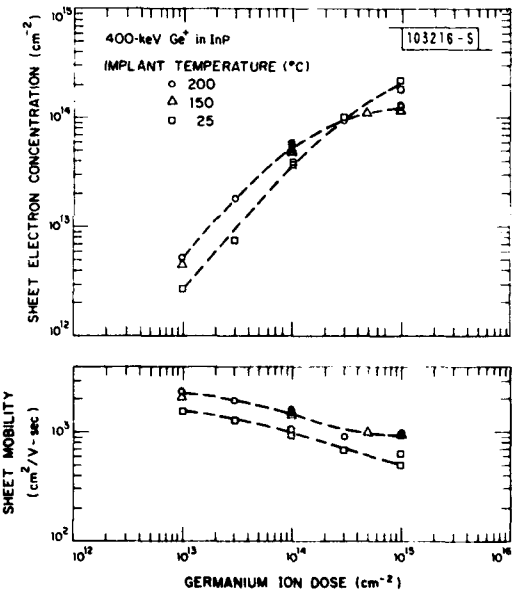

Fig. III-2. The sheet carrier concentrations and mobilities vs dose of InP samples implanted with 400-keV Ge at several temperatures, from room temperature to 200°C.

ples implanted with 400-keV Ge^+ at several temperatures between room temperature and 200°C are plotted. For doses less than 10^{14} cm^{-2}, the sheet carrier concentration and mobility vary qualitatively with implant temperature as indicated in Fig. III-1. For doses of 3×10^{14} cm^{-2}, the measured sheet carrier concentrations are essentially equal for samples implanted at room temperature and 200°C, while for doses of 1×10^{15} cm^{-2} the concentrations in the samples implanted at room temperature [(1.8 to 2.2) × 10^{13} cm^{-2}] were higher than those measured on samples implanted at 150° and 200°C [(1.2 to 1.3) × 10^{14} cm^{-2}]. The sheet mobilities, however,

are considerably higher on the samples implanted at elevated temperatures so that the sheet resistivities of all the samples implanted with 1×10^{15} cm^{-2} are about 55 Ω/□.

Similar behavior at high doses also has been observed with Si and Sn. For 400-keV Si doses of 1×10^{15} cm^{-2}, samples implanted at room temperature had sheet carrier concentrations and mobilities of about 4.0×10^{14} cm^{-2} and 780 cm^2/V-sec for a sheet resistivity of 20 Ω/□. Similar samples implanted at 200°C had sheet concentrations, mobilities, and resistivities of 2.8×10^{14} cm^{-2}, 1500 cm^2/V-sec, and 15 Ω/□, respectively.

To examine the effects of implant temperature and dose on the spatial distribution of the electrical active implanted ions, several samples were selected for depth profiling using a series of Hall measurements combined with step etching.[22] Figure III-3 shows the carrier concentration and mobility vs depth for several InP samples implanted with 400-keV Si at room temperature and 200°C and doses of 1×10^{14} and 1×10^{15} cm^{-2}. Also plotted are the theoretical Si profiles for doses of 1×10^{14} and 1×10^{15} cm^{-2} which were calculated using the Johnson and Gibbons formulation of LSS theory.[23,24]

The sample implanted at room temperature with 1×10^{14} cm^{-2} had a sheet concentration and mobility of 4.9×10^{13} cm^{-2} and 1600 cm^2/V-sec, respectively. This sheet carrier

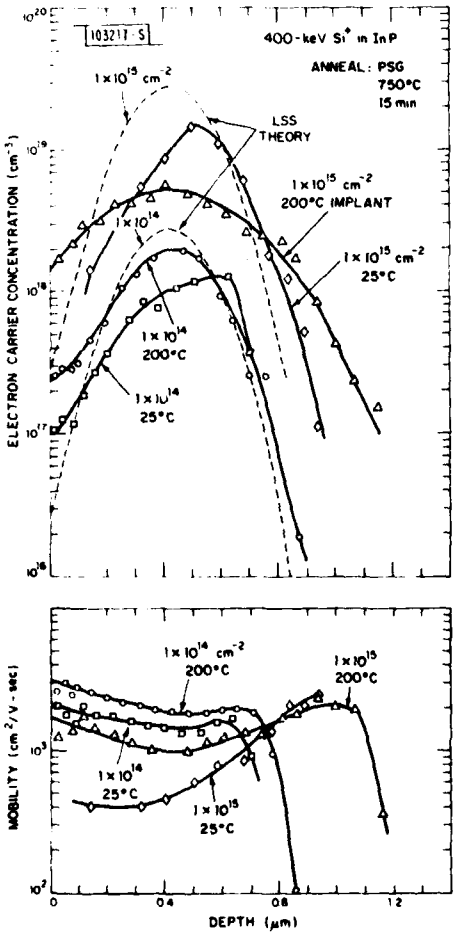

Fig. III-3. The carrier concentrations and mobilities vs depth of InP samples implanted with 400-keV Si at 25° and 200°C and with doses of 1×10^{14} and 1×10^{15} cm^{-2}. Also shown are the expected profiles calculated from the LSS range theory.

concentration value is on the low end of the values observed on room-temperature implanted samples [see Fig. III-1(b)], while the mobility is on the high end. This sample was chosen since it is believed that in it residual n-type damage effects are minimal and will have little effect on the measured profile. As shown in Fig. III-3, the sample has a carrier concentration near the surface which is substantially lower than expected, indicating that the implanted Si in this region is either not electrically active or compensated.

For the sample implanted at 200°C with 1×10^{14} cm^{-2} of Si, the carrier-concentration profile more nearly fits that expected from LSS theory. The measured peak carrier concentration is 2×10^{18} cm^{-2} at a depth of about 0.44 μm, which is only slightly deeper than the depth expected from LSS theory. Inclusion of higher-order moments in this range theory would probably result in even better agreement with the experimental data. The mobility for this sample implanted at 200°C is higher than that observed on the sample implanted at room temperature for all depths. The decrease in mobility in the deep tail of the profile is believed to be due to a decrease in the screening factor;[25] which results in an increase in the ionized impurity scattering from the deep levels in the Fe-doped substrate.

For the sample implanted at 200°C with 1×10^{15} cm^{-2} of Si, the peak of the measured carrier concentration is also about where it would be expected from range theory. The distribution, however, is much wider than expected indicating that substantial diffusion of the implanted Si has taken place. Samples implanted at room temperature with 1×10^{15} cm^{-2} showed a higher peak carrier concentration than the sample implanted at 200°C, but, as with the lower-dose room-temperature implant, the concentration in the region from the surface past the calculated peak is much lower than expected, again indicating that the implanted Si in this region is not electrically active or compensated. The mobility of the higher-dose room-temperature implanted sample is lower than that of the similar sample implanted at 200°C. It appears, therefore, that even for high doses, heated implants will generally be more desirable.

J. P. Donnelly
G. A. Ferrante

IV. GROWTH-TEMPERATURE DEPENDENCE OF LATTICE MISMATCH IN LPE GaInAsP/InP

Lattice matching is an important condition for GaInAsP/InP double heterostructure lasers and avalanche photodiodes. In the LPE growth of a GaInAsP layer on an InP substrate, the composition and lattice parameter of the epitaxial layer have been known to be functions of the growth temperature.[26,27] In this work, we report the measured growth temperature dependence of the GaInAsP/InP lattice mismatch over a wide range of quaternary compositions.

The substrates were n-type (Sn-doped, $n \sim 1 \times 10^{17}$ cm^{-3}), $\langle 100 \rangle$-oriented, and polished InP wafers. A constant growth temperature was used for each LPE run. The substrate was first etched by a pure In-melt for 10 sec, then slid under the GaInAsP growth solution. The room-temperature lattice mismatch between the grown GaInAsP layer (generally 1 to 5 μm thick) and the underlying InP substrate was determined by X-ray diffraction.

Figure IV-1 shows an example of the X-ray results. The lattice mismatch, $\Delta a/a$, was obtained from the shift, $\Delta(2\theta)$, of the diffraction maxima, based on Bragg's equation, $2a \sin\theta = m\lambda$, with $m = 6$ and $\lambda = 1.5406$ Å. For a given GaInAsP growth solution, a different growth temperature resulted in a different $\Delta a/a$. Figure IV-2 shows the growth-temperature dependence of $\Delta a/a$ obtained for a growth-solution composition which produces $\lambda_Q = 1.31$ μm at $\Delta a/a = 0$ (λ_Q is the wavelength corresponding to the energy gap of the quaternary layer). The data points in Fig. IV-2 fall approximately on a straight line. One straight line of this kind was obtained for each of eight different solution compositions used in this work. In Fig. IV-3 the slopes of these straight lines are plotted vs the corresponding λ_Q's.

In this work $(1/a)(\partial a/\partial T) \simeq -5 \times 10^{-4}$/°C has been observed for $1.3 \lesssim \lambda_Q \lesssim 1.55$ μm. This implies that precise temperature control to better than 2°C is necessary for a good lattice-matched GaInAsP/InP heterostructure. Feng et al.[27] have reported $(1/a)(\partial a/\partial T) = -2 \times 10^{-4}$/°C for $\lambda_Q = 1.15$ μm, which is 67 percent of the corresponding value in Fig. IV-3. We believe that the present value is more reliable, because our measurement was based on larger $|\Delta a/a|$'s and, therefore, had smaller errors due to signal overlap.

Figure IV-3 shows that $-(1/a)(\partial a/\partial T)$ rises almost linearly from zero for the wavelength region $0.92\ \mu m \leq \lambda_Q \leq 1.15\ \mu m$. This behavior can be understood from the fact that, for those compositions, Ga and As are dilute species both in the growth solution and in the epitaxial layer. A similar argument applies to the drop of $-(1/a)(\partial a/\partial T)$ for $\lambda_g \rightarrow 1.67$ μm, where the P concentration approaches zero.

In this work, smooth GaInAsP layers have been grown directly on InP substrates without an intervening InP buffer layer. However, a buffer layer is needed for a smoother GaInAsP/InP interface in DH lasers. We have recently observed some effect of the InP buffer layer on the subsequent GaInAsP growth. Details of these experiments will be reported at a later time.

Z-L. Liau D. E. Mull
J. J. Hsieh J. N. Walpole
T. A. Lind

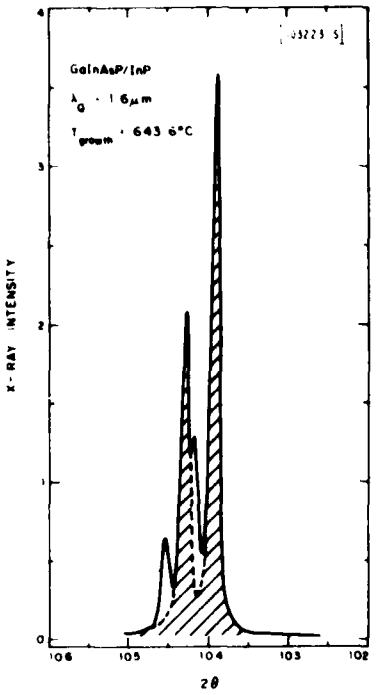

Fig. IV-1. Intensity distribution of an X-ray beam after being diffracted by a GaInAsP/InP heterostructure. The two shaded peaks are the diffraction maxima due to the InP substrate and correspond to the wavelength doublet in the primary X-ray beam ($CuK_{\alpha 1}$ and $CuK_{\alpha 2}$). Overlapped with the shaded peaks are the diffraction maxima due to the GaInAsP layer (~7 μm thick). The Δa/a corresponding to the relative shift between the two sets of maxima is -15.9×10^{-4}.

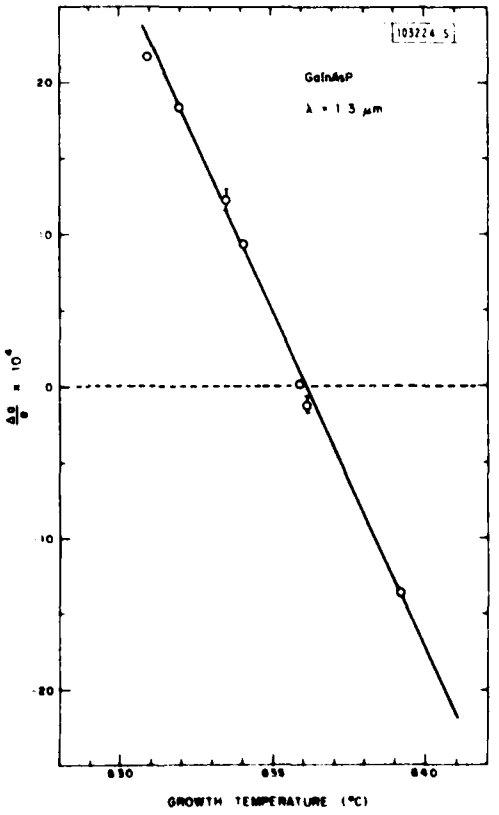

Fig. IV-2. LPE GaInAsP/InP lattice mismatch as a function of growth temperature.

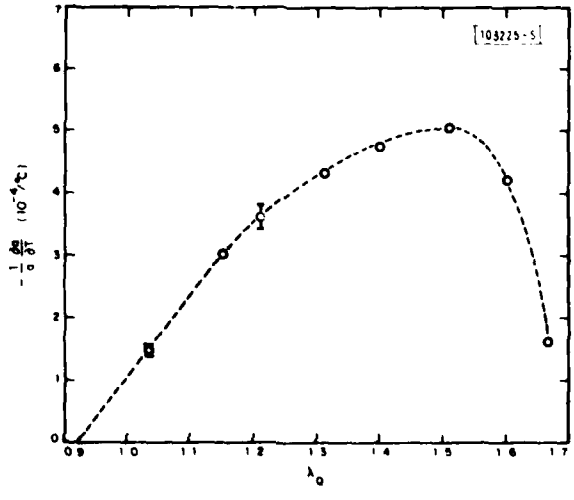

Fig. IV-3. The negative of the growth-temperature derivative of the GaInAsP/InP lattice mismatch as a function of λ_Q.

REFERENCES

1. T. Miya, Y. Terumura, T. Hosaka, and T. Miyashita, Electron. Lett. 15, 106 (1979).
2. H. Kawaguchi, K. Takahei, Y. Toyoshima, H. Nagai, and G. Iwane, Electron. Lett. 15, 669 (1979).
3. S. Akiba, K. Sakai, Y. Matsushima, and T. Yamamoto, Electron. Lett. 15, 606 (1979).
4. _____, 5th European Conf. on Optical Communication, Amsterdam, The Netherlands, 17-19 September 1979. Although these authors state that η_d = 19 percent/facet for the diode whose light output vs current curve is given in their Fig. 2, the value of η_d obtained from this curve is 19 percent for both facets.
5. I. P. Kaminow, R. E. Nahory, M. A. Pollack, L. W. Stulz, and J. C. DeWinter, Electron. Lett. 15, 763 (1979).
6. J. J. Hsieh, IEEE J. Quantum Electron. QE-15, 694 (1979), DDC AD-A076459.
7. _____, Appl. Phys. Lett. 28, 283 (1976), DDC AD-A025631/3.
8. J. J. Hsieh and C. C. Shen, Fiber Integ. Opt. 1, 357 (1978).
9. C. A. Armiento, S. H. Groves, and C. E. Hurwitz, Appl. Phys. Lett. 35, 333 (1979), DDC AD-A076467; also Semiannual Technical Summary on Electrooptical Devices, Lincoln Laboratory, M.I.T. (31 March 1979), p. 11, DDC AD-A077152.
10. Semiannual Technical Summary on Electrooptical Devices, Lincoln Laboratory, M.I.T. (30 September 1979), p. 7, DDC AD-A084410.
11. K. Nishida, K. Taguchi, and Y. Matsumoto, Appl. Phys. Lett. 35, 251 (1979).
12. C. E. Hurwitz and J. J. Hsieh, Appl. Phys. Lett. 32, 487 (1978), DDC AD-A060752/3.
13. R. Yeats and S. H. Chiao, Appl. Phys. Lett. 34, 581 (1979).
14. J. P. Donnelly and C. E. Hurwitz, Appl. Phys. Lett. 31, 418 (1977), DDC AD-A050856; also Semiannual Technical Summary on Electrooptical Devices, Lincoln Laboratory, M.I.T. (30 September 1977), p. 11, DDC AD-A054477/5; (31 March 1978), p. 7, DDC AD-A059062/0; (30 September 1978), p. 9, DDC AD-A069091/7; and (30 September 1979), p. 11, DDC AD-A084410.
15. D. E. Davies, J. P. Lorenzo, and T. G. Ryan, Solid-State Electron. 21, 981 (1978).
16. W. T. Devlin, K. T. Ip, D. P. Leta, L. F. Eastman, and G. H. Morrison, in Gallium Arsenide and Related Compounds (St. Louis) 1978, C. M. Wolfe, Ed. (The Institute of Physics, London, 1979), Conf. Ser. 45, p. 510.
17. J. P. Donnelly and C. A. Armiento, Appl. Phys. Lett. 34, 96 (1979).
18. D. E. Davies, W. D. Potter, and J. P. Lorenzo, J. Electrochem. Soc. 125, 1845 (1978).
19. D. E. Davies, J. J. Comer, J. P. Lorenzo, and T. G. Ryan, Appl. Phys. Lett. 35, 142 (1979).
20. B. K. Shin, Appl. Phys. Lett. 29, 438 (1976).
21. J. S. Harris, in Ion Implantation in Semiconductors, I. Ruge and J. Grasl, Eds. (Springer-Verlag, Berlin, 1971), p. 157.
22. J. D. Sansbury and J. F. Gibbons, Radiat. Eff. 6, 269 (1970).
23. W. J. Johnson and J. F. Gibbons, Projected Range Statistics in Semiconductors (Stanford University Bookstore, Stanford, California, 1970); also J. F. Gibbons, W. T. Johnson, and S. W. Mylroie, Projected Range Statistics (Halsted Press, New York, 1975).
24. J. Lindhard, M. Scharff, and H. Schiott, K. Dan. Vidensk. Selsk. Mat.-Fys. Medd. 33, 1 (1963).

25. See for example: R. H. Smith, Semiconductors (Cambridge University Press, Cambridge, 1959), p. 151.

26. J. J. Hsieh, M. C. Finn, and J. A. Rossi, Chapter 1 in Gallium Arsenide and Related Compounds (St. Louis) 1976, L. F. Eastman, Ed. (The Institute of Physics, London, 1977), Conf. Ser. 33b, p. 37, DDC AD-A046985/8.

27. M. Feng, L. W. Cook, M. M. Tashima, T. H. Windhorn, and G. E. Stillman, Appl. Phys. Lett. 34, 292 (1979).

UNCLASSIFIED

SECURITY CLASSIFICATION OF THIS PAGE *(When Data Entered)*

REPORT DOCUMENTATION PAGE	READ INSTRUCTIONS BEFORE COMPLETING FORM
1. REPORT NUMBER: ESD-TR-80-168	2. GOVT ACCESSION NO.: AD-A092 699
	3. RECIPIENT'S CATALOG NUMBER
4. TITLE *(and Subtitle)*: Electrooptical Devices	5. TYPE OF REPORT & PERIOD COVERED: Semiannual Technical Summary, 1 October 1979 – 31 March 1980
	6. PERFORMING ORG. REPORT NUMBER
7. AUTHOR(s): Charles E. Hurwitz	8. CONTRACT OR GRANT NUMBER(s): F19628-80-C-0002
9. PERFORMING ORGANIZATION NAME AND ADDRESS: Lincoln Laboratory, M.I.T., P.O. Box 73, Lexington, MA 02173	10. PROGRAM ELEMENT, PROJECT, TASK AREA & WORK UNIT NUMBERS: Program Element Nos. 62702F and 61102F; Project Nos. 2306 and 4600
11. CONTROLLING OFFICE NAME AND ADDRESS: Rome Air Development Center, Griffiss AFB, NY 13440	12. REPORT DATE: 31 March 1980
	13. NUMBER OF PAGES: 24
14. MONITORING AGENCY NAME & ADDRESS *(if different from Controlling Office)*: Electronic Systems Division, Hanscom AFB, Bedford, MA 01731	15. SECURITY CLASS. *(of this report)*: Unclassified
	15a. DECLASSIFICATION DOWNGRADING SCHEDULE

16. DISTRIBUTION STATEMENT *(of this Report)*

Approved for public release; distribution unlimited.

17. DISTRIBUTION STATEMENT *(of the abstract entered in Block 20, if different from Report)*

18. SUPPLEMENTARY NOTES

None

19. KEY WORDS *(Continue on reverse side if necessary and identify by block number)*

electrooptical devices	proton bombardment	ion implantation
avalanche photodiodes	double-heterostructure	GaInAsP/InP lasers

20. ABSTRACT *(Continue on reverse side if necessary and identify by block number)*

This report covers work carried out with support of the Department of the Air Force during the period 1 October 1979 through 31 March 1980. A part of this support was provided by the Rome Air Development Center.

CW operation at temperatures up to 55°C has been achieved for GaInAsP/InP double-heterostructure (DH) lasers emitting at 1.5 μm, which were grown without a GaInAsP buffer layer. These devices are of interest for use as sources in fiber-optics communications systems, since the lowest transmission loss reported for fused-silica optical fibers occurs at 1.55 μm.

Surface passivation techniques developed for InP and GaInAsP avalanche photodiodes have resulted in reductions of dark current as large as four orders of magnitude, to values as low as 1.6 × 10⁻⁶ A/cm²

DD FORM 1 JAN 73 1473 EDITION OF 1 NOV 65 IS OBSOLETE

UNCLASSIFIED

SECURITY CLASSIFICATION OF THIS PAGE *(When Data Entered)*

20. ABSTRACT (Continued)

at 0.9 V_b, where V_b is the breakdown voltage. Devices consisting entirely of InP have been passivated with plasma-deposited Si_3N_4, and those with a GaInAsP layer but with the p-n junction in InP have been passivated with polyimide. Neither of these techniques successfully reduces dark currents in devices with the p-n junction in the GaInAsP, but a film of photoresist sprayed with SF_6 as the propellant has given excellent results.

The electrical characteristics of InP ion implanted with Sn, Ge, Si, and C have been investigated. All of these column IV elements yielded n-type conductivity and Sn, Ge, and Si showed high electrical activation; however, implanted C was found to have a net electrical activation of only about 5 percent.

The growth-temperature dependence of the GaInAsP/InP lattice mismatch has been measured over a wide range of quaternary compositions. Smooth GaInAsP layers have been grown directly on InP substrates without an InP buffer layer; however, the use of an InP layer results in a smooth GaInAsP/InP interface, which is needed for DH lasers.